

design of a better annealing schedule and, hence, more accurate structures.

Evidently the capacity of these Hamiltonians per residue is significantly larger than it is for Ising neural networks per spin (2, 3). The energies of the final annealed structures are sufficiently close to those obtained by annealing the x-ray structure of the target protein that rms values less than 3.0 Å are secured for most calculations. The number of protein families being small—of order 20 to 40 (19)—one has hope that a cunningly chosen database would have sufficient capacity to classify proteins into these families.

The Hamiltonian can also recognize variant sequences as demonstrated in the last entry of Table 1 and in Fig. 1C. The *Desulfovibrio vulgaris* rubredoxin differs from the *Clostridium pasteurianum* form included in the database at 50% of the residues. Of these, six are not synonymous in terms of our simple hydrophobicity scale. The 2.5 Å rms value demonstrates the Hamiltonian is able to generalize to this degree of substitutional mutation.

The large capacity of this simple associative memory Hamiltonian and its modest ability to generalize with respect to site mutations suggest that this approach offers a fruitful perspective on tertiary structure recognition. As it stands, the associative memory approach should be considered as a framework (as opposed to a method) for predicting structures. The recall of structure is, however, comparable or better than earlier studies that used only hydrophobicity statistics (20), which give rms values of 4 to 8 Å, although this is a somewhat unfair comparison. Further features must be incorporated in a fully predictive associative-memory Hamiltonian. Structures which have been modified by insertions and deletions must also be recognized. This requires a consideration of the invariances of Hamiltonians to these sequence transformations. The role of vector charges, many-body interactions, and modifications of the interaction network, such as dilution or changing the range of the potentials, are also of interest.

REFERENCES AND NOTES

1. M. Levitt and A. Warshel, *Nature* **253**, 694 (1975); J. Skolnick, A. Kolinski, R. Yaris, *Proc. Natl. Acad. Sci. U.S.A.* **85**, 5057 (1987); N. Go, *Annu. Rev. Biophys. Bioeng.* **12**, 183 (1983); H. Wako and H. A. Scheraga, *J. Protein Chem.* **1**, 85 (1982).
2. J. J. Hopfield, *Proc. Natl. Acad. Sci. U.S.A.* **79**, 2554 (1982).
3. D. J. Amit, H. Gutfreund, H. Sompolinsky, *Phys. Rev. Lett.* **55**, 1530 (1985).
4. D. L. Stein, *Proc. Natl. Acad. Sci. U.S.A.* **82**, 3670 (1985).
5. D. Poland and H. A. Scheraga, *Theory of Helix-Coil Transitions in Biopolymers* (Academic Press, New York, 1970).
6. J. D. Bryngelson and P. G. Wolynes, *Proc. Natl. Acad. Sci. U.S.A.* **84**, 7524 (1987).

7. T. Garel and H. Orland, *Europhys. Lett.* **6**, 307 (1988); *ibid.*, p. 597; E. I. Shakhnovich and A. Gutin, *ibid.* **8**, 3271 (1988); *J. Phys. A* **22**, 1647 (1989).
8. N. Qian and T. J. Sejnowski, *J. Mol. Biol.* **202**, 865 (1988).
9. L. H. Holley and M. Karplus, *Proc. Natl. Sci. Acad. U.S.A.* **86**, 152 (1989).
10. T. R. Kirkpatrick and P. G. Wolynes, *Phys. Rev. B* **36**, 8552 (1987).
11. B. Derrida, *Phys. Rev. Lett.* **45**, 79 (1980).
12. J. D. Bryngelson and P. G. Wolynes, *J. Phys. Chem.*, in press; C. Levinthal, *J. Chim. Phys.* **65**, 44 (1968).
13. D. Eisenberg, R. M. Weiss, T. C. Terwilliger, W. Wilcox, *Faraday Symp. Chem. Soc.* **17**, 109 (1982).
14. D. Eisenberg, R. M. Weiss, T. C. Terwilliger, *Proc. Natl. Acad. Sci. U.S.A.* **81**, 140 (1984); M. Shiffer and A. B. Edmundson, *Biophys. J.* **7**, 121 (1967); J. Palan and P. Puigdomenech, *J. Mol. Biol.* **88**, 457 (1974); V. I. Lim, *ibid.*, p. 857; *ibid.*, p. 873.
15. I. D. Kuntz, *J. Am. Chem. Soc.* **94**, 4009 (1972).
16. R. Staden, *Nucleic Acids Res.* **10**, 2951 (1982).
17. S. Kirkpatrick, C. D. Gelatt, Jr., M. P. Vecchi, *Science* **220**, 671 (1983).
18. R. Srinivasan *et al.*, *J. Mol. Biol.* **98**, 739 (1975).
19. J. S. Richardson, *Adv. Protein Chem.* **34**, 167 (1981).
20. M. Ycas, N. S. Goel, J. W. Jacobsen, *J. Theor. Biol.* **72**, 443 (1978); N. S. Goel and M. Ycas, *ibid.* **77**, 253 (1979); I. D. Kuntz, G. M. Crippen, P. A. Kollman, *Biopolymers* **18**, 939 (1979).
21. We thank J. Bryngelson, H. Frauenfelder, J. Onuchic, K. Schulten, Z. Schulten, and J. Widom for helpful discussions, and D. Evensky and Z. Schulten for help with the graphics. Supported by NSF grant CHE 84-18619; the computations were done at the National Center for Supercomputer Applications, Urbana, Illinois.

9 June 1989; accepted 13 September 1989

Styles of Volcanism on Venus: New Arecibo High Resolution Radar Data

DONALD B. CAMPBELL, JAMES W. HEAD, ALICE A. HINE, JOHN K. HARMON, DAVID A. SENSKE, PAUL C. FISHER

Arecibo high-resolution (1.5 to 2 km) radar data of Venus for the area extending from Beta Regio to western Eüsila Regio provide strong evidence that the mountains in Beta and Eüsila Regiones and plains in and adjacent to Guinevere Planitia are of volcanic origin. Recognized styles of volcanism include large volcanic edifices on the Beta and Eüsila rises related to regional structural trends, plains with multiple source vents and a mottled appearance due to the ponding of volcanic flows, and plains with bright features surrounded by extensive quasi-circular radar-dark halos. The high density of volcanic vents in the plains suggests that heat loss by abundant and widely distributed plains volcanism may be more significant than previously recognized. The low density of impact craters greater than 15 km in diameter in this region compared to the average density for the higher northern latitudes suggests that the plains have a younger age.

VOLCANISM IS ONE OF THE FUNDAMENTAL processes of heat transfer from planetary interiors (1). The location of volcanic deposits and edifices, their volumes, and their sequence provide evidence for quantitative assessments of heat transfer in space and time. The nature of volcanic deposits provides clues to the style of volcanism, which is related to composition, volatile content, interaction with the crust during ascent, and the structure of the crust and lithosphere (2). New data for about 32×10^6 km² of the equatorial region of Venus (7% of the surface area of the planet) (Fig. 1) provide higher quality images than previously available for this region because of significant improvement in sensitivity and increased resolution by a factor of

5 to 10 for more than 50% of the region. They provide information about the nature of volcanic deposits and permit comparison to other parts of Venus previously imaged at both high and low resolution. These new data show that volcanism is an extremely widespread process in this part of Venus and that volcanic deposits cover most of the surface area and occur in a variety of environments and styles.

Observations of Venus were made during the summer of 1988 with the 12.6-cm wavelength Arecibo radar facility, and data were obtained with resolutions between 1.5 and 2 km. A circularly polarized signal was transmitted, and both senses of received circular polarization were recorded. The equatorial region was viewed at incidence angles from about 12° to 60° (the extremes encompass only a small fraction of the area, and the incidence angle for most of the coverage was between 20° and 50°, similar to the range expected for the Magellan mission), and the signal-to-noise ratio decreased with increasing incidence angle because of both the

D. B. Campbell, National Astronomy and Ionosphere Center, Cornell University, Ithaca, NY 14853.
J. W. Head, D. A. Senske, P. C. Fisher, Department of Geological Sciences, Brown University, Providence, RI 02912.
A. A. Hine and J. K. Harmon, National Astronomy and Ionosphere Center, Arecibo Observatory, Arecibo, Puerto Rico 00612.

decrease in backscatter cross section and increased atmospheric absorption. Twenty-five "looks" (estimates of the backscatter cross section) were averaged to form the images. This area was chosen for the initial data reduction and analysis because its latitude range, 12°N to 45°N, overlapped the southern edge of the coverage from the Venera 15/16 spacecraft by about 10° (3) and extended the coverage another 23° toward the equator. It also provides overlap with earlier lower resolution Earth-based radar studies (4) and with Pioneer Venus radar images (5).

The data cover an area extending from just west of Beta Regio (270° longitude) across Guinevere Planitia to the eastern extent of western Eisila Regio (10°) and include the central part of Guinevere Planitia and, north of Eisila, the southern part of Sedna Planitia (Fig. 1). Beta and Eisila Regiones, rising up to several kilometers above mean planetary radius, form part of the equatorial highlands (6) that stretch almost completely around the circumference of Venus (7). The lowlands of Guinevere Planitia, lying below mean planetary radius, are the only major zone of lowlands disrupting the generally continuous equatorial highlands (Fig. 1).

Beta Regio is a large topographic rise that is characterized by the convergence of several rift zones, the most distinctive of which, Devana Chasma, is oriented generally north-south (Fig. 1). Geologic relations indicate

that thermal uplift, rifting, and associated volcanism are prominent in this area (8-10) and that it is similar to several other regions identified as tectonic junctions in the equatorial highlands (11). Earlier analyses have suggested that rifting and volcanism are intimately interrelated (8). In the case of Rhea Mons, volcanic construction appears to have predated the major rifting, whereas for Theia Mons, volcanism largely followed rifting, forming a large construct along the western edge of the rift and filling in the rift zone (8-10). The new images reveal that Theia Mons is located where three or more major rift zones intersect (Fig. 2, A and B) and that extensive faulting cuts the central part of the volcano in a zone 60 to 100 km wide and oriented about N10°E. The orientation of this fault zone is different from the generally N30°-40°E trend of the braided lineaments of Devana Chasma just north of Theia, and the fault zone generally bisects the trend of the two southern arms of the rift zone. This relation may indicate that extension on the various rift arms has not been synchronous, but rather that it occurred in different parts of the rift, with different orientations, at different times. The shape of the dark, central caldera-like structure is apparently controlled by this zone of faulting. We interpret the central dark deposits to be relatively smoother or lower reflectivity summit lava flows that have erupted in and adjacent to the caldera and flowed along structurally controlled fault

zones to produce this elongate deposit parallel to the general fault zone.

The detailed configuration of the Theia Mons deposits and their relation to the rift zones are also clear. A broad, generally circular bright deposit 300 to 400 km in diameter surrounds the irregularly shaped central dark structure. It is centered on the butterfly-shaped flanking deposits that are arranged bilaterally about the strike of the rift zone. The stratigraphic relations for Theia Mons can be seen in terms of the map patterns of the deposits: the broad butterfly shape of the deposits to the northwest and southeast represent volcanic material emplaced on the flanks of the rift zone, but where the flanks of Theia slope into the rift zones, a more complex relation is seen. The gentle slopes strongly suggest that lava from the volcano has been emplaced in this area, but much of the surface is dominated by younger faults. In several places, particularly to the northeast of Theia, zones of flows from Theia can be seen to be superposed on the more intensely faulted rift interior (A in Fig. 2B). On the basis of these relations, we conclude that volcanism and rifting are intimately interrelated in the evolution of the volcano and the interior of the rift zone and that extension was a continuous process throughout the evolution of Beta Regio.

Eisila Regio is a prominent linear highland 1000 to 3000 km wide trending generally west-northwest, extending some 10,000 km west from Aphrodite Terra, and rising up to about 1.5 km above mean planetary radius. Classified as an upland rise (5, 11), Eisila Regio generally lacks the distinctive rift zones characteristic of Aphrodite to the east and Beta to the west; it is characterized by a series of mountains (Sif, Gula, Sappho, and others) situated on or near the summits of the broad rises (5). The data show that Sif Mons, in westernmost Eisila Regio, is a central volcano whose deposits form a 400- to 600-km-wide edifice, rising some 1.5 km above Eisila Regio (Figs. 1 and 2, C and D).

Sif Mons is characterized by a classical shield volcanic form in plan view, with a central circular feature about 50 km in diameter from which radiate a series of radar-bright, elongate, lobate features interpreted to be lava flows or flow complexes. These flow units are generally 20 to 30 km wide and 100 to 150 km in length, but some are up to 400 to 600 km long. Their orientation is in many cases controlled by topographic slope (for example, flow unit A in Fig. 2, C and D).

Although the tectonic structure in this upland rise (5, 11, 12) is not nearly as well developed as that in Beta, there is evidence for some structural control of deposits. For example, there is a northwest to southeast

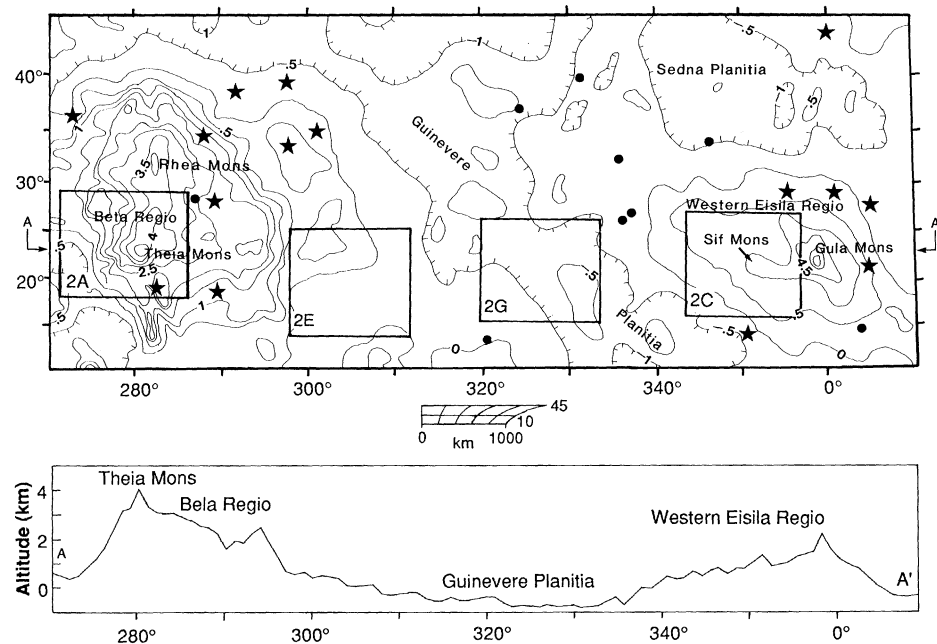
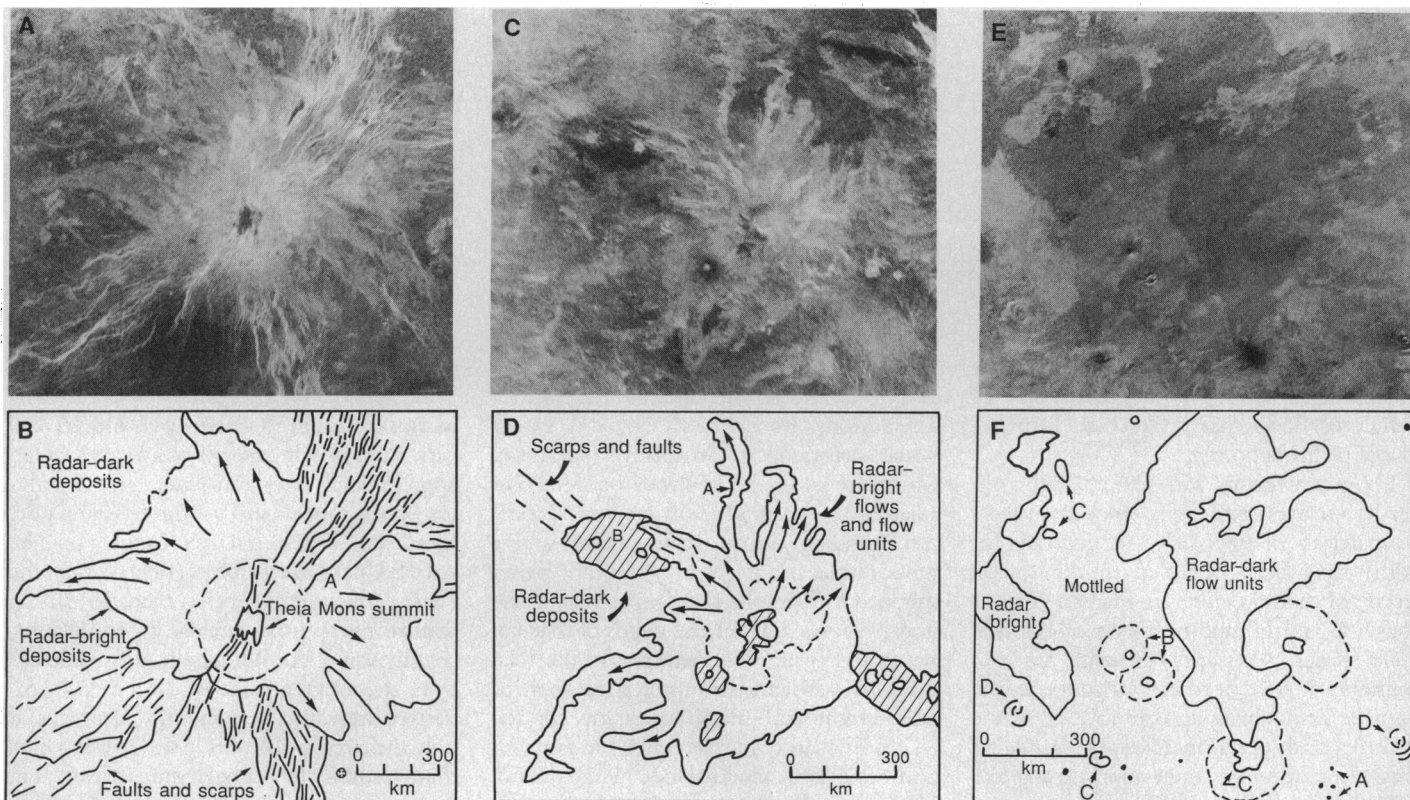


Fig. 1. Location and contour map of the Beta Regio–Western Eisila Regio area. Contours are derived from Pioneer Venus altimetry data (5) and are at 0.5-km intervals. Boxes show locations of areas of detailed analysis illustrated in Fig. 2. Topographic profile (A-A') across region is shown at the base. Location of circular features of probable impact origin (stars) and possible impact origin (filled circles) are shown.



trend to the topography of Western Eüsila (Fig. 1), and the two linear dark deposits (B and C in Fig. 2D) and the summit of Sif Mons are located and aligned along this trend. In addition, the deposits of Sif are asymmetrically distributed in a butterfly-like arrangement, and deposits to the northeast and southwest are texturally different. Structures appear to be oriented en echelon along the dominant trend (Fig. 2, C and D), somewhat similar to those observed farther east in the equatorial highlands in Western Aphrodite Terra.

A number of small radar-bright features with surrounding radar-dark areas, interpreted to be volcanic sources and deposits, occur aligned along a northwest-southeast axis and on the flanks of the volcano. Sif Mons clearly has contributed some lava fill to the surrounding plains, but the abundance of individual volcanic sources in the lowlands, the great distances involved, and the concentration of deposits within about 400 km of Sif suggests that most of the fill is from other sources.

The plains of Guinevere Planitia lie at, or just below, mean planetary radius and are regionally flat (Figs. 1 and 2, E and F). The plains are characterized, particularly in the western areas of Guinevere, by (i) abundant apparent volcanic sources vents (5 to 20 km in diameter) and (ii) broad regions of mottled bright and dark deposits representing widespread and superposed flows that origi-

nated from the source vents. These two characteristics also distinguish the plains from the edifice deposits. There is a wide variety of source vents (letters in Fig. 2F) including (i) small domes less than 25 km in diameter, (ii) domes and complex craters superposed on broad shields 100 to 200 km in diameter, (iii) distinct and diffuse dark deposits from 25 to 50 km in diameter, and (iv) concentric arcs forming centers about 50 km in diameter. The dark deposits and arcs appear to be located on local rises or shields in many areas, but the low topography makes exact determination of elevations impossible with available data. An extensive radar-dark flow unit (Fig. 2, E and F) probably consists of multiple flows from several sources; one flow emanates from the vicinity of a diffuse dark deposit 50 km across that appears, on the basis of its form, to be centered on a 200-km-wide dome or shieldlike structure. The density of vents identified in a 2.3×10^6 km² area in Fig. 2C is about 12 to 15 per 10^6 km². The mottling observed in the plains is clearly related to embaying and overlapping flows and flow units characterized by different surface roughness or dielectric properties, or both. The causes of the differences in radar backscatter (such as differences in composition, surface flow texture, age, or mantling, for example) and their absolute magnitude are not known. In the overall region imaged, there does not appear to be a consistent

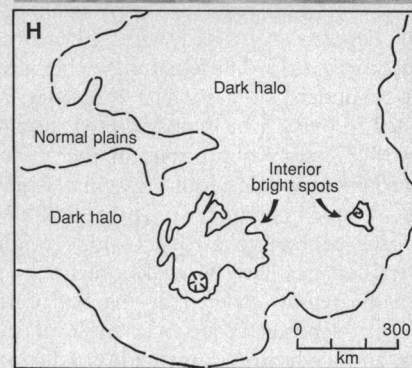
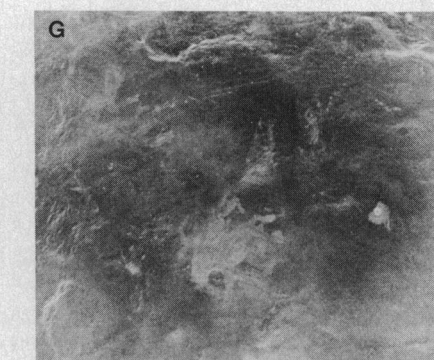


Fig. 2. Arcibo radar images and geological sketch maps. (A) and (B) South-central Beta Regio, showing Devana Chasma and Theia Mons and rift-related edifice volcanism; (C) and (D) Western Eüsila Regio, showing Sif Mons and central edifice volcanism; (E) and (F) Southwestern Guinevere Planitia, showing mottled plains and abundant volcanic sources; (G) and (H) South-central Guinevere Planitia, showing dark-halo plains. Letters point out features identified in text.

relation between youth and radar backscatter cross section. In some places the relatively youngest flows appear dark (Fig. 2, E and F), while in others (for example, Theia and Sif) many of the youngest flows are bright (Fig. 2, A and C). The generally mottled nature of the plains is clearly a result of the ponding of flows and flow deposits in regions of low slopes, relative to the more distinctive flows seen in many areas of the steeper flanks of the isolated edifices. The general style of volcanism is similar to plains volcanism on Earth (13), in which abundant small shields and vents are the source of numerous flows that coalesce to form regional plains deposits.

Irregular deposits with extremely low radar backscatter (indicating smooth surfaces or materials of low dielectric constant, or both) have been observed in the lowest terrain of central Guinevere Planitia (Figs. 1 and 2, G and H) and northeast of Western Eisila Regio (4). Such deposits are also common at low northern latitudes in the Pioneer Venus imaging data (5, 14). These dark deposits occur in relatively low-lying areas. In addition to their anomalously low radar backscatter, these areas, which range in width from 300 to 1000 km, are characterized by diffuse boundaries with the surrounding plains and an interior radar bright spot that typically displays a craterlike morphology with associated bright deposits. These central features and their halos could be either impact craters or volcanic craters and surrounding deposits (5, 15). We tentatively interpret the central bright spots in Fig. 2G to be of volcanic origin on the basis of the size of the extensive bright deposits relative to that of the crater and their flow-lobe like nature, as compared to other craters interpreted to be of impact origin on Venus (15). The dark halos may be smooth flow deposits associated with the central structure, but the diffuse nature of the outer halo boundary suggests that they may be related to pyroclastic deposits, even though explosive volcanic eruptions in the Venus environment would require magmas with a high volatile content (16). Three dark-halo deposits containing a total of nine bright central features have been identified.

In the region covered by the new data, volcanic deposits occur over most of the area, and we have documented two distinct associations and styles of volcanism. In edifice volcanism (Theia and Sif Mons), large 200- to 600-km-wide volcanic constructs occur on regional topographic rises, and the location of the edifice is closely linked to regional structural and topographic trends; the majority of the volcanism occurs at or near the central part of the edifice. The structural and topographic control of the

edifice deposits commonly results in a butterfly-like array of deposits. In the case of Theia, there has been a constant interplay between rifting and volcanism. Sif Mons appears more isolated but is associated with an echelon structures along the linear crest of Western Eisila Regio, and it may represent an earlier stage of evolution of volcanism and rifting compared to Beta Regio. These volcanic edifices, which are clearly associated with topographic rises that may be related to larger scale mantle anomalies, appear to dominate the volcanic activity and output in the region and, in the case of Theia Mons, are intimately linked to extensional deformation. In plains volcanism, which occurs in the lowlands between and adjacent to Beta and Eisila Regiones, there are abundant source vents. These source vents display a variety of styles, are rather subdued topographically, and are characterized by flows and related deposits that coalesce and overlie one another in the relatively flat lowlands to produce the mottled radar-bright and -dark appearance of the plains. The large number and wide distribution of vents in the lowlands (12 to 15 per 10^6 km²) strongly suggest that plains volcanism is an important aspect of surface evolution and contributed to heat loss on Venus, in addition to the topographic rises and localized central edifices (such as Beta and Theia, and western Eisila and Sif).

Individual flow units and the mottled nature of the plains are much more apparent in these data than in Venera 15 and 16 data for much of the northern high latitudes (17). The moderate radar illumination characteristic of the Arecibo viewing geometry and incidence angles (12° to 60°) enhances the detection of variations in surface roughness relative to the lower incidence angles characteristic of the Venera 15 and 16 systems (3). This difference may account for some of the differences in images, although additional study of the regions where the two data sets overlap is required. The detection of individual flows and flow units at the incidence angles of the recent Arecibo data indicates that data from the upcoming Magellan mission, where incidence angles will be in the same range, will be extremely useful in the study of volcanic deposits and stratigraphy.

In all, 127 probable impact craters with diameters greater than 15 km have been identified in the Venera 15 and 16 data for the northernmost quarter of the planet's surface (15). Seven of these fall within the coverage of the new Arecibo data, and a comparison of the images of these seven craters for the different incidence angles of the two radars provides a model for the identification of probable impact (or, at least, the same type of) craters in the Areci-

bo data. Approximately 24 circular features of possible impact origin and with diameters >15 km have been identified (black circles and stars in Fig. 1). However, less than half of them have a general appearance similar to the probable impact craters in the Venera data. Virtually all of these (stars in Fig. 1) are located on the margins of Beta and Eisila Regiones whereas most of the remaining features (black circles in Fig. 1) are located on the plains.

Estimates of the mean crater retention age of the northernmost quarter of the surface of Venus based on the number of probable impact craters in the Venera 15 and 16 data vary from about 150 million years (18) to approximately 1 billion years (15), depending on the model used for the cratering rate. If all 24 of the circular features in the Arecibo data are impact craters, then the density of craters greater than 15 km in diameter is approximately 0.7 per 10^6 km², slightly lower but not significantly different from the average value of 1.1 per 10^6 km² derived from the Venera data. However, if only the circular features in the Arecibo data that resemble the probable impact craters in the Venera data are counted, then the density is less than 0.4 per 10^6 km², significantly less than that for the more northerly regions and indicative of a younger surface. The absence of these most likely candidates for impact craters in the volcanic plains may imply that the surface is very young or that the radar signatures of impact craters in the volcanic plains and on the margins of the rises are different.

REFERENCES AND NOTES

1. S. C. Solomon and J. W. Head, *J. Geophys. Res.* **87**, 9236 (1982).
2. L. Wilson and J. W. Head, *Nature* **302**, 663 (1983).
3. Yu. N. Aleksandrov *et al.*, *Sov. Sci. Rev. E Astrophys. Space Phys.* **6**, 61 (1988).
4. D. B. Campbell and B. A. Burns, *J. Geophys. Res.* **85**, 8271 (1980).
5. G. H. Pettengill *et al.*, *ibid.*, p. 8261; D. Senske, thesis, Brown University, Providence, RI (1989).
6. R. J. Phillips, W. M. Kaula, G. E. McGill, M. C. Malin, *Science* **212**, 879 (1981).
7. J. W. Head, L. C. Crumpler, P. C. Fisher, *Lunar Planet. Sci.* **XIX**, 475 (abstr.) (1988).
8. G. E. McGill, S. J. Steenstrup, C. Barton, P. G. Ford, *Geophys. Res. Lett.* **8**, 737 (1981).
9. D. B. Campbell, J. W. Head, J. K. Harmon, A. A. Hinc, *Science* **226**, 167 (1984).
10. E. R. Stofan *et al.*, *Geol. Soc. Am. Bull.* **101**, 143 (1989).
11. D. A. Senske and J. W. Head, *Lunar Planet. Sci.* **XX**, 986 (abstr.) (1989).
12. ——— *ibid.*, p. 984 (abstr.).
13. R. Greeley, in *Volcanism of the Eastern Snake River Plain, Idaho*, NASA Comparative Planetary Geology Guidebook, R. Greeley and J. King, Eds. (National Aeronautics and Space Administration, Washington, DC, 1977), pp. 24–44.
14. G. H. Pettengill *et al.*, *Science* **205**, 90 (1979).
15. B. A. Ivanov *et al.*, *J. Geophys. Res.* **91**, D413 (1986). A. T. Basilevsky *et al.*, *ibid.* **92**, 12,869 (1987).
16. J. W. Head and L. Wilson, *ibid.* **90**, 6873 (1986).
17. V. L. Barsukov *et al.*, *ibid.* **91**, D378 (1986).

18. G. G. Schaber, E. M. Shoemaker, R. C. Kozak, *Astron. Vestnik* **21**, 144 (1987).
19. The National Astronomy and Ionosphere Center is operated by Cornell University under a cooperative agreement with the National Science Foundation and with support from the National Aeronautics and Space Administration (NASA). This research was also supported by grants from the Planetary Geology and Geophysics and the Planetary Astronomy Programs of the Solar System Exploration Division of NASA to D.B.C. and J.W.H. We thank personnel at the Arecibo Observatory and students and staff in the Brown University Planetary Geology Group for assistance.

16 May 1989; accepted 28 August 1989

Movement Protein of Tobacco Mosaic Virus Modifies Plasmodesmatal Size Exclusion Limit

SHMUEL WOLF, CARL M. DEOM, ROGER N. BEACHY, WILLIAM J. LUCAS

The function of the 30-kilodalton movement protein (MP) of tobacco mosaic virus is to facilitate cell-to-cell movement of viral progeny in an infected plant. A novel method for delivering non-plasmalemma-permeable fluorescent probes to the cytosol of spongy mesophyll cells of tobacco leaves was used to study plasmodesmatal size exclusion limits in transgenic plants that express the MP gene. Movement of fluorescein isothiocyanate-labeled dextran (F-dextran) with an average molecular mass of 9400 daltons and an approximate Stokes radius of 2.4 nanometers was detected between cells of the transgenic plants, whereas the size exclusion limit for the control plants was 700 to 800 daltons. No evidence of F-dextran metabolism in the leaves of the transgenic plants was found. Thus, the tobacco mosaic virus movement protein has a direct effect on a plasmodesmatal function.

PLASMODESMATA ARE NARROW strands of cytoplasm that penetrate adjoining cell walls to interconnect plant cells, thus forming a community of living protoplasts termed the symplasm. Cells and tissues that are remote from direct sources of nutrients can be nourished by the movement of carbohydrates, amino acids, and inorganic ions through plasmodesmata. Plasmodesmata also represent potential pathways for the passage of signals, either electrical or hormonal, which could integrate and regulate the activities of different parts of the symplasm (1).

The function of the symplasmic pathway in tissues and organs of diverse plant species has been reported (2). Techniques for microinjection of nontoxic membrane-impermeable fluorescent dyes (for example, Lucifer yellow CH), used extensively for tracing neurological interactions (3) and studying gap junctions (4), have been used in a number of plant tissues (2, 5-7). Synthesis of fluorescent peptide probes of known molecular mass and radius, developed to probe the size exclusion limits of gap junctions (8), has also been exploited by plant scientists to establish the extent of symplasmic permeability in plant tissues (2, 5-9).

Certain types of plant viruses spread

throughout the host by moving through plasmodesmata, as in the case of mosaic viruses (10-12). Electron microscopic evidence of viral particles moving through plasmodesmata of a variety of plants has been reported (11, 13). Virus gene expression, therefore, may provide a system for studying plasmodesmata as well as virus movement (14, 15).

Conclusive evidence that the 30-kD movement protein (MP) of tobacco mosaic virus (TMV) is involved in cell-to-cell movement of the virus was demonstrated by Deom *et al.* (14). Expression of the MP gene in transgenic plants complemented the Ls1 mutant of TMV, a mutant that is tempera-

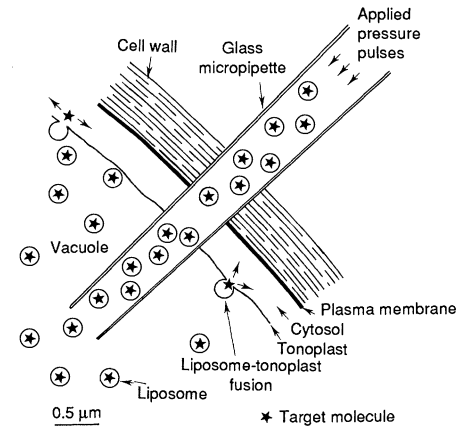


Fig. 1. Schematic representation of the technique employed to introduce fluorescently labeled target molecules, *in vivo*, into the cytosol of tobacco mesophyll cells. Lucifer yellow CH (LYCH; Sigma) and FITC-labeled hexaglycine (F-Gly₆) and dextrans with molecular masses of 3,900, 9,400, and 17,200 daltons were used as fluorescent probes and were prepared as described by Simpson (17). Liposomes were prepared by the freeze-thaw method described by Pick (18) as modified by Madore *et al.* (5) and were back-loaded via capillary action into the tips of glass micropipettes having a tip diameter of 0.5 to 1.0 μm. The capillary was sealed into a micropipette holder equipped with a luer port, and pressure was controlled by a Pneumatic PicoPump (World Precision Instruments, model PV830). Injection pressure was 7 to 15 psi. Pipette movement for cell impalement was controlled by a hydraulically driven micromanipulator (Narishige model MO-102).

ture-sensitive (ts) in cell-to-cell movement (16). In transgenic plants infected with Ls1 and maintained at the nonpermissive temperature, cell-to-cell movement of the Ls1 virus was potentiated in both inoculated and upper systemic leaves. Although this finding provides direct evidence that the MP of TMV is necessary for virus movement, little is known about the mode by which the MP facilitates movement. We now show that the expression of the TMV MP gene in trans-

Table 1. Mobility of fluorescent probes through the symplasmic pathway of mesophyll cells of transformed tobacco plants. Data are presented as the percentage of injections that showed movement of the specific probe, as determined 2 min after injection. (Values in parentheses represent number of injections).

| Probe* | Molecular mass (daltons) | Transgenic plant line | MP genotype | Percentage of injections expressing movement |
|--------------------|--------------------------|-----------------------|-----------------|--|
| LYCH | 457 | 277 | MP ⁺ | 100 (5) |
| | | 306 | MP ⁻ | 100 (5) |
| F-Gly ₆ | 749 | 277 | MP ⁺ | 100 (8) |
| | | 306 | MP ⁻ | 50 (10) |
| F-Dextran | 3,900 | 277 | MP ⁺ | 100 (6) |
| | | 306 | MP ⁻ | 14 (7) |
| F-Dextran | 9,400 | 277 | MP ⁺ | 93 (15) |
| | | 306 | MP ⁻ | 0 (12) |
| F-Dextran | 17,200 | 277 | MP ⁺ | 0 (6) |
| | | 306 | MP ⁻ | 0 (6) |

*Described in Fig. 1.

S. Wolf and W. J. Lucas, Botany Department, University of California, Davis, CA 95616.
C. M. Deom and R. N. Beachy, Department of Biology, Washington University, St. Louis, MO 63130.